Science of the Total Environment 812 (2022) 152270

Contents lists available at ScienceDirect

Science of the Total Environment

journal homepage: www.elsevier.com/locate/scitotenv

Investigating the sources of atmospheric nitrous acid (HONO) in the megacity of Beijing, China

Rongrong Gu [a,b], Hengqing Shen [a,*], Likun Xue [a,*], Tao Wang [b,a,*], Jian Gao [c], Hong Li [c], Yutong Liang [b,1], Men Xia [b], Chuan Yu [a], Yiming Liu [d], Wenxing Wang [a,c]

[a] Environment Research Institute, Shandong University, Qingdao 266237, China
[b] Department of Civil and Environmental Engineering, The Hong Kong Polytechnic University, Hong Kong 99907, China
[c] State Key Laboratory of Environmental Criteria and Risk Assessment, Chinese Research Academy of Environmental Sciences, Beijing 100012, China
[d] School of Atmospheric Sciences, Sun Yat-sen University, Zhuhai 519082, China

HIGHLIGHTS

- The HONO/NO_x ratio in early summer is twice that in winter in urban Beijing.
- Heterogeneous reaction of NO_2 on the ground governs HONO formation in early summer.
- Homogeneous reaction of NO + •OH is the dominant source of HONO in winter.
- HONO is the major precursor of primary •OH in both early summer and winter.

GRAPHICAL ABSTRACT

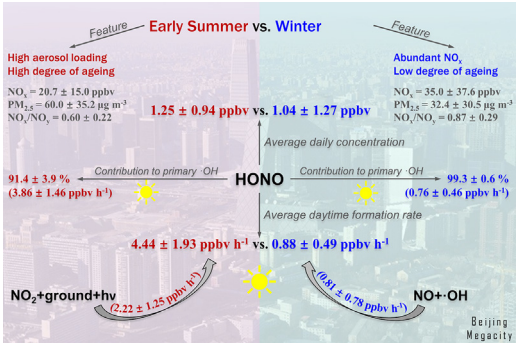

ARTICLE INFO

Article history:
Received 1 September 2021
Received in revised form 2 December 2021
Accepted 4 December 2021
Available online 10 December 2021

Editor: Jianmin Chen

Keywords:
Nitrous acid (HONO)
Seasonal variation
Budget analysis
Hydroxyl radical (•OH)
Atmospheric oxidation capacity

ABSTRACT

Nitrous acid (HONO) can powerfully influence atmospheric photochemistry by producing hydroxyl radical (•OH), which is a crucial oxidant that controls the fate of atmospheric trace species. To deduce HONO formation mechanisms in polluted regions, two field observations were conducted in urban Beijing during the early summer of 2017 and the winter of 2018. These two seasons bore distinguishing pollution characteristics with a higher degree of ageing and heavier aerosol loading in the early summer and more abundant NO_x (NO_x = NO + NO_2) in the winter. Elevated concentrations of HONO were observed during these two seasons, with the mean ± standard deviation (maximum) concentrations of 1.25 ± 0.94 (6.69) ppbv and 1.04 ± 1.27 (9.55) ppbv in early summer and winter, respectively. The observed daytime (08:00–17:00 h, local time) HONO production rate was several times higher in early summer than in winter (4.44 ± 1.93 ppbv h^{-1} vs. 0.88 ± 0.49 ppbv h^{-1}). Budget analysis revealed distinct daytime HONO formation mechanisms during these two seasons. Photo-induced heterogeneous conversion of NO_2 on the ground surface dominated in early summer, and homogeneous reaction of NO + •OH was dominant in winter. Photolysis of HONO was the major source of primary •OH in both seasons, and thus, played a key role in the regulation of atmospheric oxidising capacity. This study demonstrates the significant seasonal variations in HONO budget and underlines the predominant role of HONO in primary •OH production in Beijing. Our findings will be helpful to gain an understanding of the chemical mechanisms underlying the formation of secondary pollution in metropolitan areas.

* Corresponding authors.
E-mail addresses: hqshen@sdu.edu.cn (H. Shen), xuelikun@sdu.edu.cn (L. Xue), tao.wang@polyu.edu.hk (T. Wang).
[1] Now at Department of Environmental Science, Policy and Management, University of California, Berkeley, CA 94720-3110, USA.

http://dx.doi.org/10.1016/j.scitotenv.2021.152270

1. Introduction

Nitrous acid (HONO) can strongly affect tropospheric chemistry by photo-dissociating to hydroxyl radicals (•OH) (Kleffmann and Gavriloaiei, 2005; Xue et al., 2016). As one of the most crucial atmospheric oxidising agents, •OH controls the removal of trace species and dominates the formation of secondary pollutants, and thus, profoundly influences air quality and climate (Gligorovski et al., 2015). The photolysis of HONO can significantly contribute to primary •OH formation throughout the day, with the average contributions being >90% in winter and ranging from 50% to 80% in summer (Aumont et al., 2003; Elshorbany et al., 2010; Fu et al., 2019; Jiang et al., 2020). Therefore, identification of HONO sources is essential for a comprehensive understanding of the underlying atmospheric chemistry.

Decades of investigations have uncovered various processes that contribute to HONO under certain atmospheric conditions: direct emissions (e.g., soil and fuel combustion emissions) (Kurtenbach et al., 2001; Liang et al., 2017; Oswald et al., 2013; Sun et al., 2020; Yokelson et al., 2009), homogeneous reactions (e.g., NO + •OH and NO_2^* + •OH) (Li et al., 2008; Zhang et al., 2016), photosensitive heterogeneous reactions (conversion of NO_2 on various surfaces, such as ground, aerosol, buildings, vegetation, ocean, and so on) (Arens et al., 2001; Ma et al., 2017; Stemmler et al., 2006; Stutz et al., 2002; Wen et al., 2019), and photolysis of N-containing compounds with high oxidation states (e.g., particulate nitrate [pNO_3], HNO_3/nitrate adsorbed on surfaces, and nitrophenols) (Barsotti et al., 2017; Bejan et al., 2006; Ye et al., 2016; Ye et al., 2017). However, HONO budgets are yet to be understood in many environments. On the one hand, significant uncertainties in almost all HONO formation mechanisms limit the quantification of HONO sources, hindering our understanding of its budgets. These uncertainties arise from insufficient measurement accuracies, undetermined reaction rates, and wide-ranging uptake efficiencies of precursors (Liu et al., 2019a; Xue et al., 2020). On the other hand, a dearth of integrated studies that combine comprehensive field observations with detailed budget analysis in different atmospheric chemical environments further impedes our understanding of HONO sources and the role of HONO in atmospheric oxidation.

In most previous studies on HONO source tracking, the homogeneous reaction of NO with •OH was identified as a relatively minor contributor, while the heterogeneous conversion of NO_2 on surfaces has widely been highlighted as a predominant HONO source. Kleffmann and Gavriloaiei (2005) found an order of magnitude of discrepancy between the observed and calculated HONO concentrations, in a forest environment, when only pure gas phase mechanisms were considered in the calculation. Large gaps between the observed HONO source strength and that calculated from the NO + •OH reaction have also been commonly found in urban (Hao et al., 2020; Li et al., 2018), suburban (Michoud et al., 2014; Yang et al., 2014), rural (Su et al., 2008; Tsai et al., 2018), mountainous (Jiang et al., 2020; Zhou et al., 2007), and coastal regions (Meusel et al., 2016; Yang et al., 2021). In recent years, unexpectedly high •OH concentrations have been detected in megacities, even during the winter, with a maximum value of $>10^6$ molecules cm^{-3} (Kanaya et al., 2007; Tan et al., 2018). The coexistence of high concentration of •OH and large amount of NO, which is released by intensive anthropogenic activities, suggests that the importance of the NO + •OH reaction in HONO formation needs to be reexamined under this condition. In addition, although the heterogeneous conversion of NO_2 on surfaces has been commonly regarded as a crucial HONO formation path, on which surface the heterogeneous reaction dominates is still under debate. The two surfaces of ground and aerosol are recognized significant in urban environments and draw the most attention; when some studies emphasized the prominent role of the ground surface (VandenBoer et al., 2013; Zhang et al., 2016), some others argued the significance of the aerosol surface (Liu et al., 2014; Zhang et al., 2020). Therefore, it is necessary to explore the roles of ground and aerosol in heterogeneous NO_2 conversion to HONO.

To estimate the budgets and impacts of HONO in polluted urban areas, we performed two field campaigns during the early summer of 2017 and the winter of 2018 in urban Beijing. Beijing is located in one of the most polluted regions in China (Fig. 1a–b), and thus, frequently experiences heavy aerosol loading and high concentrations of nitrogen oxides (NO_x, i.e., NO + NO_2). We investigated seasonal variations in HONO and HONO budgets under two contrasting pollution conditions. We also analysed the impacts of HONO on the atmospheric oxidant •OH. Our work presents the distinct seasonal variations in HONO characteristics and sources, underlines the significant role of the NO + •OH reaction in HONO formation, and highlights the overwhelming contribution of HONO to primary •OH across seasons in Beijing.

2. Experiments

2.1. Study site and time

Field measurements were performed on the rooftop of a three-storey building (approximately 12 m above the ground) in the Chinese Research Academy of Environmental Sciences (CRAES, 40.04°N, 116.42°E), outside the north Fifth Ring Road of Beijing in North China (Fig. 1a–c). The CRAES is located in a typical urban area, surrounded by dense urban traffic and crowded residential and commercial buildings but few industrial pollution sources. As substantial anthropogenic pollutants are emitted in the megacity of Beijing (Fig. 1a–b), severe air pollution is frequently observed in this region. We conducted field measurements during 7–30 May 2017 and 15–30 January 2018. During these two periods, prevailing southerly winds bring pollutants from the downtown (Fig. 1c–d), which strengthened the representativeness of our observation site for urban Beijing. For more information about the study site, previous studies by Wang et al. (2010) and Xia et al. (2019) are recommended.

2.2. Measurements

Trace gases, aerosols, and meteorological parameters were measured online during the comprehensive field experiments. The trace species were sampled with roof-across inlets and detected by household instruments. Meteorological parameters were measured in situ above the rooftop. Generally, the air pollution concentrations in Beijing were high enough for sufficiently accurate detection. A brief description of the measurement instruments and methods is given below. Detailed introductions can be found in our previous studies (Gu et al., 2020; Wang et al., 2003; Xia et al., 2019; Xue et al., 2016).

2.2.1. Trace gases

Nitrous acid (HONO) was detected by a commercial long path absorption photometer (LOPAP 03, QUMA, Germany) using the photometric detection method (Heland et al., 2001). Nitric oxide (NO) and all reactive nitrogen compounds (NO_y) were measured by gas-phase chemiluminescence detection using a total reactive nitrogen oxides analyser (Model EC9843, Ecotech, Australia), which was equipped with a MoO catalytic converter. Nitrogen dioxide (NO_2) was measured by a chemiluminescence analyser (Model 42i-TL, Thermo Scientific, USA) equipped with a photolytic converter (Blue Light Converter, Meteorologie Consult GmbH, Germany) (Xu et al., 2013). Ozone (O_3) was detected by a UV photometric analyser (Model 49i, Thermo Scientific, USA). Sulphur dioxide (SO_2) was measured with a pulsed UV fluorescence gas analyser (Model 43C, Thermo Scientific, USA). Data for all of the above gases were collected with a time resolution of 1 min, except for HONO, which had a time resolution of 30 s.

2.2.2. Aerosols

$PM_{2.5}$ mass concentrations were automatically measured by a continuous particulate monitor (Model BAM 1020, Met One Instruments, USA) using the industry-proven principle of beta ray attenuation. A wide-range particle spectrometer (WPS, Model 1000XP, MSP, USA) was used to detect the dry-state particle size distribution ranging from 10 nm to 10 μm. Assuming that all of the particles were spherical, the aerosol surface area per volume of air (S/V) was estimated. Real-time concentrations of water-soluble ions in $PM_{2.5}$ (K^+, Na^+, Ca^{2+}, Mg^{2+}, NH_4^+, NO_3^-, SO_4^{2-}, and Cl^-) were

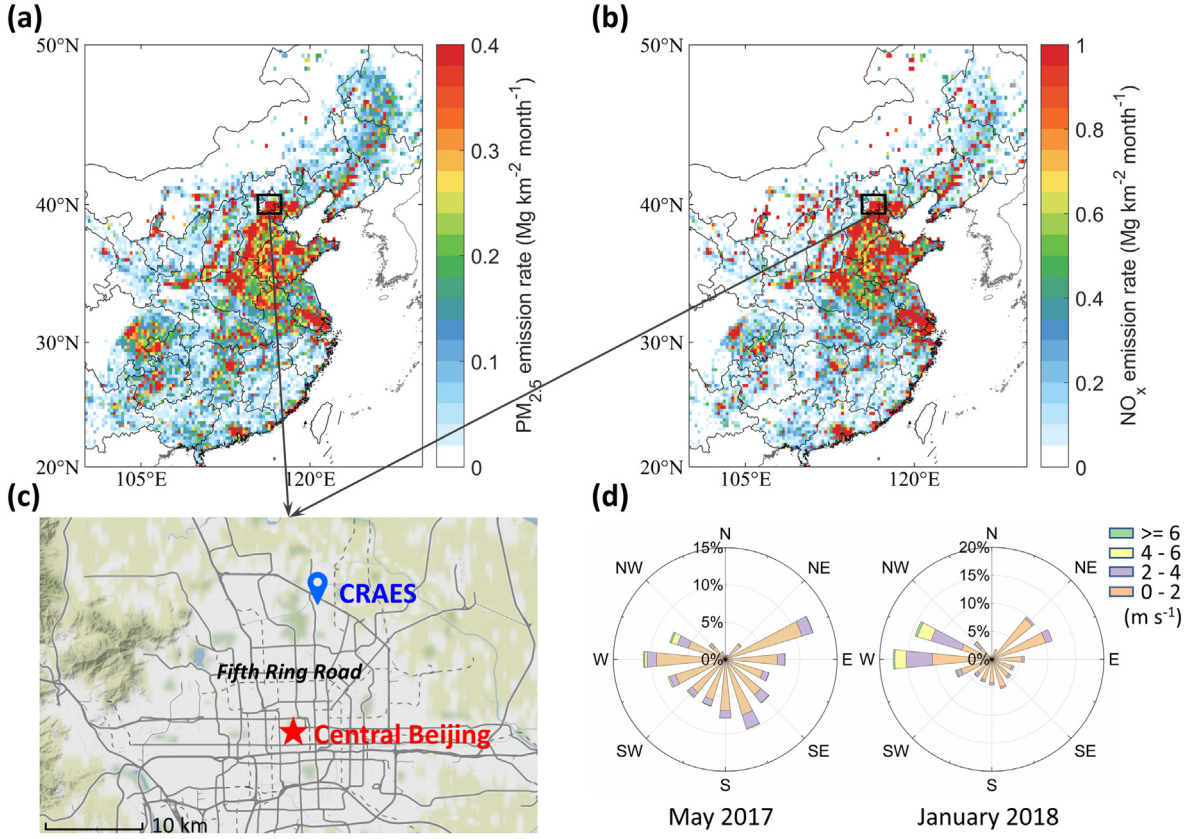

Fig. 1. Spatial distributions of (a) anthropogenic primary $PM_{2.5}$ emissions and (b) anthropogenic primary NO_x emissions in 2016 (data from the MIX emission inventory in the MEIC database of Tsinghua University, http://meicmodel.org/), (c) location of the observation site CRAES in Beijing, and (d) wind roses at the observation site during the two observation campaigns in the early summer of 2017 and the winter of 2018.

autonomously measured by the monitor for aerosols and gases (MARGA, Metrohm, Switzerland). The data were acquired at a time resolution of 5 min for $PM_{2.5}$ and S/V and 1 h for ions.

2.2.3. Meteorological parameters

Temperature (Temp), relative humidity (RH), wind speed (WS), wind direction (WD), and solar radiation (SR) were monitored by an automatic weather station (MAWS301, Vaisala, Finland). The photolysis frequency of NO_2 ($j(NO_2)$) was monitored with an actinic $j(NO_2)$ filter radiometer (Meteorologie Consult GmbH, Germany). The temporal intervals of all the meteorological data were 1 min.

3. Results and discussion

3.1. Overview of observations

Fig. 2 presents the time series of observed HONO, associated trace species, meteorological parameters, and calculated j(HONO). The missing photolysis frequencies of j(HONO) and $j(O^1D)$ were calculated from $j(NO_2)$, while the missing $j(NO_2)$ data for the early summer campaign were obtained from SR (Supplement Text S1). Fig. S1b shows the average diurnal variation in •OH, which was calculated from an empirical equation (Supplement Text S1). Table 1 lists the statistical and correlation parameters of HONO and related parameters. The meteorology featured low RH (32 ± 19% vs. 23 ± 11%) and low-speed urban district-oriented prevailing winds during the two observation campaigns in early summer and winter, despite large temperature differences between the two seasons (24.9 ± 5.0 °C vs. -2.8 ± 4.6 °C).

As shown in Fig. 2 and Table 1, the ambient air in Beijing was characterised by a high degree of ageing and heavy aerosol loading in the early summer, while it exhibited freshness and abundant NO_x during the winter. The ratio of NO_x/NO_y, which is negatively related to the ageing of the air mass (Hastie et al., 1996; Wang et al., 2016; Wilson et al., 2012), distinctly illustrated a higher atmospheric ageing degree in early summer than in winter (with the value of 0.60 ± 0.22 vs. 0.87 ± 0.29). In early summer, strong solar radiation and abundant atmospheric oxidants (e.g., O_3) could cooperatively enhance the formation of secondary pollutants (e.g., pNO_3). In winter, contrastively, continuous residential heating throughout the cold season could enhance the release of fresh pollutants and the lower boundary layer height in winter would further amplify the concentration of pollutants (e.g. NO_x of 35.0 ± 37.6 ppbv in winter vs. 20.7 ± 15.0 ppbv in early summer). The $PM_{2.5}$ concentration in early summer was twice that in winter (60.0 ± 35.2 μg m^{-3} vs. 32.4 ± 30.5 μg m^{-3}). Heavy aerosol loading, coupled with considerable Ca^{2+} content (5.9 ± 7.2 μg m^{-3} in early summer vs. 0.2 ± 0.2 μg m^{-3} in winter), indicated dust pollution in early summer (Xia et al., 2019). As shown in Fig. 2, two episodes of elevated HONO concentrations were observed: Episode I in early summer and Episode II in winter. These two episodes were representatives of pollution characteristics during the two observation periods.

The concentrations of HONO were generally higher in early summer than in winter (1.25 ± 0.94 ppbv vs. 1.04 ± 1.27 ppbv). However, the severest HONO incident occurred in winter rather than early summer (with a maximum concentration of 9.55 ppbv vs. 6.69 ppbv). Similar seasonal variations of HONO in Beijing have also been observed in other studies (Liu et al., 2021; Spataro et al., 2013; Wang et al., 2017). The 2-fold HONO/NO_x ratio in early summer compared to winter (0.067 ± 0.042 vs. 0.031 ± 0.017) corroborated the enhanced HONO generation efficiency in early summer, and the relatively low HONO/NO_x in winter suggested the increased contribution of local primary emissions to ambient HONO, as the HONO/NO_x ratio is generally much smaller in freshly emitted plumes (less than 2%) than that in well-mixed ambient air (about 7%).

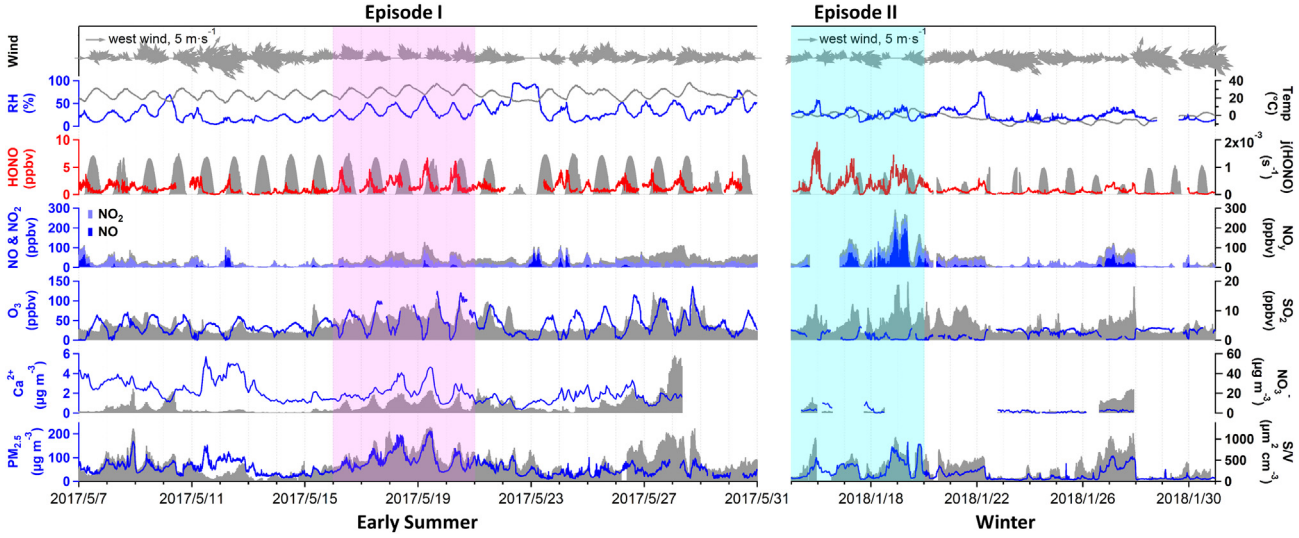

Fig. 2. Time series of the measured HONO, NO, NO_2, NO_y, O_3, SO_2, $PM_{2.5}$, Ca^{2+}, NO_3^-, aerosol surface area density (S/V), meteorological parameters (temp, RH, and wind), and the calculated *j*(HONO) during the two field campaigns in the early summer of 2017 and the winter of 2018 in Beijing.

Fig. 3 presents the average diurnal variations in HONO and related parameters. Their diurnal patterns reflect significant seasonal differences. In early summer, HONO concentration showed a typical day-fall and night-rise trend with an early morning maximum (2.33 ppbv at 06:00 h), coinciding with the diurnal patterns of NO_2. The simultaneous occurrence of an NO peak around 06:00 h indicated that heavy morning traffic might considerably contribute to HONO. In winter, the HONO concentration climbed slowly from 03:00 h and peaked at 06:00 h, then decreased to a valley at 14:00 h, afterward sharply increase to another peak (also the maximum) at 20:00 h, followed by a slight dip before 03:00 h. This wave-like diurnal variation in HONO concentration was consistent with the trend of NO_x concentration. As both NO and NO_2 were abundant and collectively accounted for 87% of NO_y, they were likely sharing the same sources with HONO or they were important HONO precursors during winter. The O_3 concentration exhibited a typical diurnal trend of increasing after sunrise, peaking around noon (12:00 h in winter vs. 14:00 h in early summer), and decreasing to a valley before dawn. The opposite diurnal trends of O_3 and HONO suggest that their contributions to atmospheric oxidising capacity change over time. $PM_{2.5}$ exhibited similar diurnal trends to those of nitrogen oxides for these two seasons. The steepest rise in $PM_{2.5}$ in the morning of early summer suggested the contribution of vehicular emission, while a sharp increase in $PM_{2.5}$ in the evenings of winter indicated the potential combined roles of fuel combustion for residential heating and boundary layer reducing. HONO/NO_x is a proper parameter to describe the heterogeneous conversion efficiency of HONO from NO_2 since the interferences of sudden air mass change could be mitigated comparing with HONO/NO_2 (Liu et al., 2019b). In winter, the diurnal pattern of HONO/NO_x was consistent with that of HONO, with a trough at 14:00 h. In early summer, however, a noontime (14:00 h) peak, also the maximum, appeared. Given the valley-like shape of the diurnal patterns of NO, NO_2, and NO_y around noon, the specific noontime peak of HONO/NO_x was ascribed to photo-enhanced HONO production. Based on the above preliminary inference, a detailed HONO budget analysis is presented in the following sections.

3.2. HONO budgets

A detailed budget analysis was carried out to estimate HONO sources and sinks under different pollution conditions in Beijing. Sources, such as direct vehicular emission, homogeneous NO + •OH reaction, (photo-induced) heterogeneous NO_2 conversion on the aerosol and ground

Table 1
Statistical and correlation parameters during the two observation campaigns in Beijing.

Parameter	Early summer						Winter					
	MIN	MED	MAX	MEAN ± SD	r1	r2	MIN	MED	MAX	MEAN ± SD	r1	r2
HONO (ppbv)	BDL	0.99	6.69	1.25 ± 0.94	1.00	0.24	BDL	0.57	9.55	1.04 ± 1.27	1.00	0.16
NO (ppbv)	BDL	0.36	72.33	2.28 ± 6.82	0.40	−0.11	BDL	1.75	196.33	12.07 ± 25.28	0.74	−0.21
NO_2 (ppbv)	0.97	15.92	63.45	18.32 ± 11.29	0.75	−0.21	1.66	19.70	74.89	22.94 ± 16.27	0.71	−0.24
NO_x (ppbv)	0.97	16.48	102.83	20.66 ± 14.98	0.73	−0.21	2.72	21.26	258.37	35.01 ± 37.65	0.83	−0.24
NO_y (ppbv)	1.02	33.73	163.61	38.48 ± 25.42	0.69	−0.04	2.02	29.83	292.67	45.36 ± 46.55	0.84	−0.22
HONO/NO_2	NA	0.064	0.839	0.072 ± 0.052	0.26	0.98	NA	0.035	0.224	0.041 ± 0.026	0.69	0.78
HONO/NO_x	NA	0.060	0.535	0.067 ± 0.042	0.24	1.00	NA	0.028	0.162	0.031 ± 0.017	0.16	1.00
NO_x/NO_y	0.07	0.57	1.00	0.60 ± 0.22	−0.08	−0.33	0.21	0.81	2.59	0.87 ± 0.29	−0.29	−0.11
O_3 (ppbv)	BDL	36	136	40 ± 25	−0.36	0.09	BDL	17	34	15 ± 10	−0.68	0.17
SO_2 (ppbv)	1.72	4.46	16.26	5.24 ± 2.69	0.20	0.03	1.57	4.04	19.84	4.94 ± 2.73	0.51	−0.23
$PM_{2.5}$ (μg m^{-3})	9.4	52.8	212.2	60.0 ± 35.2	0.41	−0.11	4.2	17.6	165.3	32.4 ± 30.5	0.65	−0.18
Ca^{2+} (μg m^{-3})	0.4	2.5	36.5	5.9 ± 7.2	0.06	0.37	BDL	0.2	1.1	0.2 ± 0.2	0.16	0.18
NO_3^- (μg m^{-3})	BDL	3.5	58.4	6.7 ± 8.4	0.31	−0.02	0.3	1.5	24.2	4.8 ± 6.3	0.31	−0.58
S/V (μm^2 cm^{-3})	11	395	1287	432 ± 275	0.40	0.02	40	242	1137	316 ± 241	0.59	−0.34
Temp (°C)	14.3	24.8	37.9	24.9 ± 5.0	−0.26	0.17	−12.6	−2.4	7.9	−2.8 ± 4.6	0.23	−0.03
RH (%)	4	28	95	32 ± 19	0.58	0.12	9	22	76	23 ± 11	0.55	0.12

Note: The parameters of r1and r2 are the correlation coefficients with HONO and HONO/NO_x, respectively; MIN, MED, MAX, MEAN, and SD refer to the minimum, median, maximum, mean, and standard deviation, respectively; BDL means below the detection limit and NA means not available. Temporal resolutions of all of the data being used are 5 min except for Ca^{2+} and NO_3^-, whose temporal resolutions were 1 h.

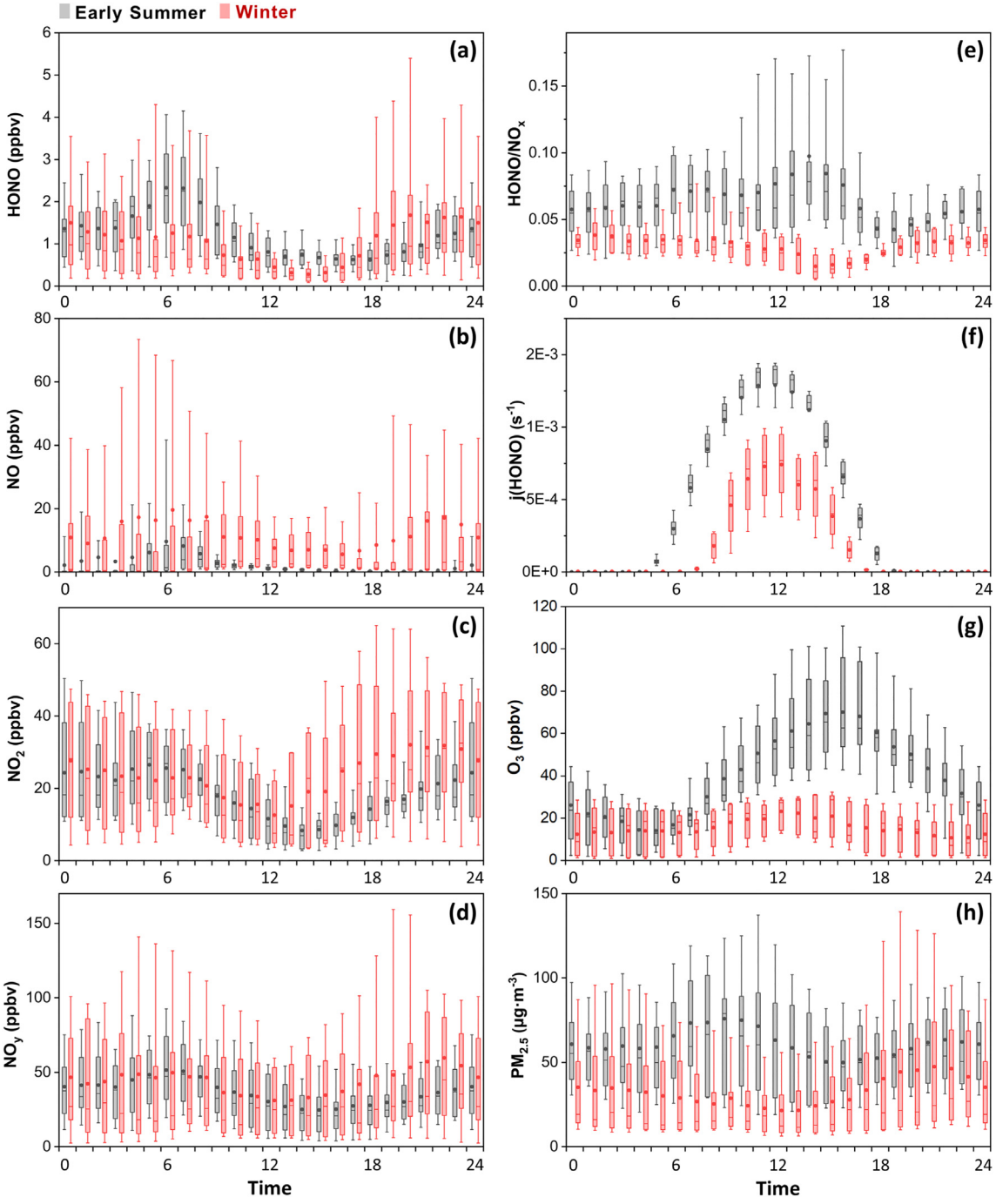

Fig. 3. Diurnal variations of (a) HONO, (b) NO, (c) NO_2, (d) NO_y, (e) $HONO/NO_x$, (f) j(HONO), (g) O_3, and (h) $PM_{2.5}$ in the early summer of 2017 and the winter of 2018 in Beijing. Box plots show the hourly data of 10%, 25%, 50%, 75%, and 90%, and the dots represent average values.

surfaces, and the photolysis of pNO_3, were taken into account. Furthermore, sinks, such as photolysis, HONO + •OH reaction, and dry deposition, were considered as well. Table 2 summarises the parameterisations used for the budget calculation. A detailed description of the sources and sinks and associated calculation methods is provided in the Supplement (Text S2).

$$P_{HONO(obs)} = L_{HONO+h\nu} + L_{HONO+\cdot OH} + L_{deposition} + \frac{\Delta HONO}{\Delta t} \quad (E1)$$

Stack plots of average diurnal sources and sinks of HONO are shown in Fig. 4. During nighttime (20:00–05:00 h), the observed production rate of HONO ($P_{HONO(obs)}$), which is defined as the sum of the total loss rates and change rates of HONO in Eq. (E1), was comparable in early summer and winter (0.58 ± 0.26 ppbv h^{-1} vs. 0.55 ± 0.45 ppbv h^{-1}). However, during daytime (08:00–17:00 h), $P_{HONO(obs)}$ in early summer was five times that in winter (4.44 ± 1.93 ppbv h^{-1} vs. 0.88 ± 0.49 ppbv h^{-1}). This large difference was consistent with the observations of approximately 2-fold HONO concentrations and j(HONO) in early summer relative to the winter (daytime average HONO of 1.02 ppbv vs. 0.54 ppbv, and j(HONO) of 1.07×10^{-3} s^{-1} vs. 4.96×10^{-4} s^{-1}). During both early summer and winter, photolysis was the major sink of HONO (89.9% vs. 78.8%, 4.11 ± 1.67 ppbv h^{-1} vs. 0.78 ± 0.45 ppbv h^{-1}), followed by dry deposition (8.3% vs. 20.2%, 0.38 ± 0.17 ppbv h^{-1} vs. 0.20 ± 0.14 ppbv h^{-1}), while the HONO + •OH reaction was negligible as a sink (1.8% vs. 1.0%, 0.08 ± 0.03 ppbv h^{-1} vs. 0.01 ± 0.01 ppbv h^{-1}).

Table 2
Parameterisations of HONO production mechanisms.

Mechanism	Parameterisation				Reference
	Parameter	Typical		Upper & lower ratio	
		Early summer	Winter		
Direct emission	*ER of HONO/NO$_x$*	0.008	0.008	$\times 2 \& \times \frac{1}{5}$	1
NO_2 on aerosol	$\gamma_{NO_2,\ aerosol}$	8.0×10^{-6}	1.2×10^{-6}	$\times 5 \& \times \frac{1}{5}$	2, 3, 4, 6
NO_2 on ground	$\gamma_{NO_2,\ ground}$	8.0×10^{-6}	1.2×10^{-6}	$\times 5 \& \times \frac{1}{5}$	2, 3, 5, 6
NO_2 on aerosol + hν	$\gamma_{NO_2,\ aerosol+h\nu}$	$1.0 \times 10^{-4} \times \frac{j(NO_2)}{j(NO_{2,\ noon})}$	$0.6 \times 10^{-4} \times \frac{j(NO_2)}{j(NO_{2,\ noon})}$	$\times 5 \& \times \frac{1}{5}$	2
NO_2 on ground + hν	$\gamma_{NO_2,\ ground+h\nu}$	$6.0 \times 10^{-5} \times \frac{j(NO_2)}{j(NO_{2,\ noon})}$	$3.8 \times 10^{-5} \times \frac{j(NO_2)}{j(NO_{2,\ noon})}$	$\times 5 \& \times \frac{1}{5}$	2
$HNO_{3\ (ads)}$ + hν	$j(HNO_{3,\ ads})$	$j(HNO_3) \times \frac{3.4\times10^{-5}}{7.0\times10^{-7}}$	$j(HNO_3) \times \frac{3.4\times10^{-5}}{7.0\times10^{-7}}$	$\times 5 \& \times \frac{1}{5}$	2, 7, 8
pNO_3 + hν	$j(pNO_{3,\ ads})$	$j(HNO_3) \times \frac{8.3\times10^{-5}}{7.0\times10^{-7}}$	$j(HNO_3) \times \frac{8.3\times10^{-5}}{7.0\times10^{-7}}$	$\times 5 \& \times \frac{1}{5}$	2, 7, 9

Note: The value of $j(NO_{2,\ noon})$ is 0.005 s^{-1}. Reference 1, Kurtenbach et al. (2001); reference 2, Liu et al. (2021); reference 3, Liu et al. (2019a); reference 4, Liu et al. (2019b); reference 5, VandenBoer et al. (2013); reference 6, Li et al. (2019); reference 7, Finlayson-Pitts and Pitts (2000); reference 8, Ye et al. (2016); reference 9, Ye et al. (2017).

The dominant HONO sources were quite different in these two seasons during the daytime. In early summer (Fig. 4a), the light-induced reactions were the major HONO formation pathways. Photo-sensitive NO_2 conversion on the ground surface, photolysis of pNO_3, and photo-induced NO_2 conversion on the aerosol surface contributed 50.0% (2.22 ± 1.25 ppbv h^{-1}), 8.4% (0.37 ± 0.31 ppbv h^{-1}), and 6.9% (0.31 ± 0.29 ppbv h^{-1}) of $P_{HONO(obs)}$, respectively. In terms of the surfaces, the ground was revealed to play a much more significant role in heterogeneous HONO formation than the aerosol, even under conditions of high aerosol loading (Fig. 4c). The contribution of the NO + •OH reaction began to rise in the early morning, reached its maximum at 07:00 h, and gradually decreased throughout the day. Despite that NO + •OH only contributed 8.1% (0.36 ± 0.24 ppbv h^{-1}) to the overall $P_{HONO(obs)}$ throughout the daytime, it was more important in the early morning, when its contribution to $P_{HONO(obs)}$ was 17.8% (0.97 ± 1.25 ppbv h^{-1}) during 06:00–09:00 h. The positive correlation between HONO and NO_2 (Fig. 5a) further indicated the significant role of NO_2 heterogeneous conversion in HONO formation as mentioned above. Higher HONO/NO_x ratios in daytime relative to nighttime, under the same RH conditions (Fig. 5b), demonstrated the effects of solar radiation on daytime HONO formation. Fig. 5b also indicated that the NO_2 conversion efficiency was influenced by RH. As RH increased from 0–10% to 60–70%, the average HONO/NO_x ratio rose from 0.056 ± 0.058 to 0.080 ± 0.012. The RH dependence of NO_2 heterogeneous conversion varied between day and night (Fig. 5b). During the nighttime, HONO/NO_x linearly tripled as RH increased from 0% to 70%. During the daytime, however, the HONO/NO_x ratio at low RH (0–20%) was comparable to that at high RH (50–60%), although HONO/NO_x linearly increased with increasing RH between 20% and 60%. As the lowest RH levels (0–20%) were observed around noon (Fig. S2), the elevated HONO/NO_x at low RH was ascribed to the strongest noontime light-enhancing effects in HONO formation.

In winter (Fig. 4b), the homogeneous NO + •OH reaction was the paramount HONO formation pathway, contributing to 51.5% (0.81 ± 0.78 ppbv h^{-1}) of the total calculated HONO production rates ($P_{HONO(cal)}$). In winter as compared with early summer, the greater than 5-fold NO concentration (12.07 ± 25.28 ppbv vs. 2.28 ± 6.82 ppbv) but only two-thirds reduction of •OH concentration ((1.32 ± 0.42) × 10^6 cm^{-3} vs. (3.40 ± 0.66) × 10^6 cm^{-3}) explains the enhanced role of NO + •OH in HONO formation (0.81 ± 0.78 ppbv h^{-1} vs. 0.36 ± 0.24 ppbv h^{-1}) in winter. Direct

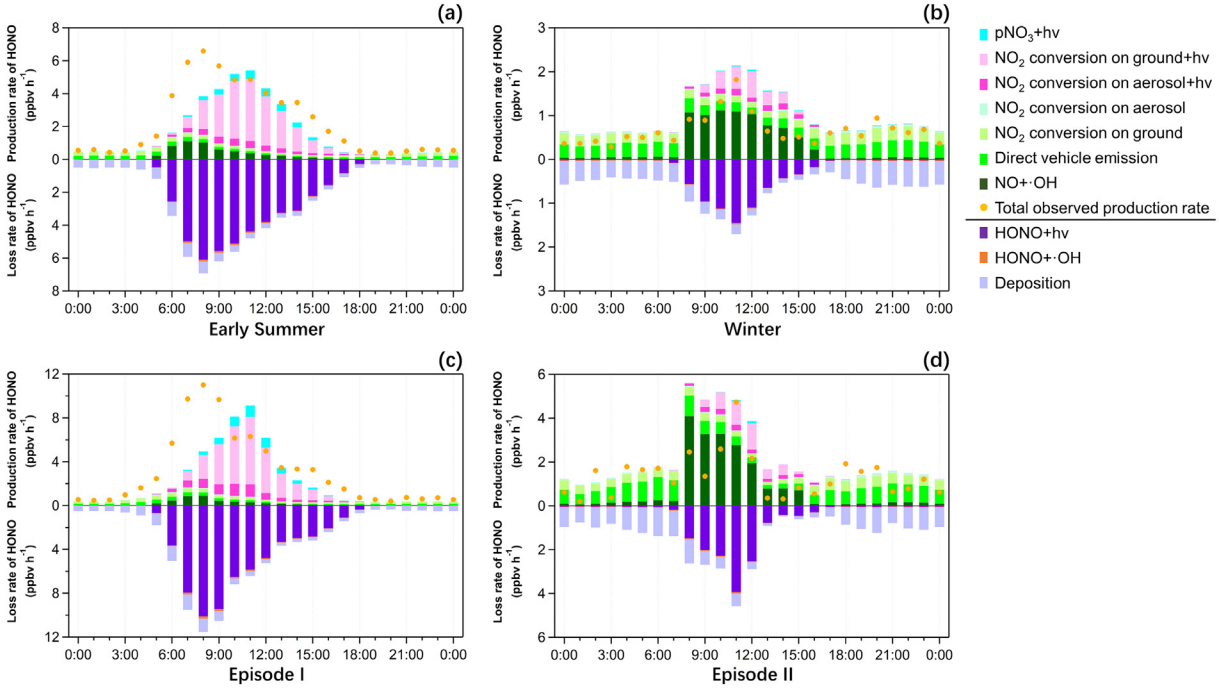

Fig. 4. Budgets of HONO in Beijing during (a) early summer, (b) winter, (c) HONO pollution Episode I in early summer (characterised by heavy aerosol loading), and (d) HONO pollution Episode II in winter (characterised by high NO_x concentration).

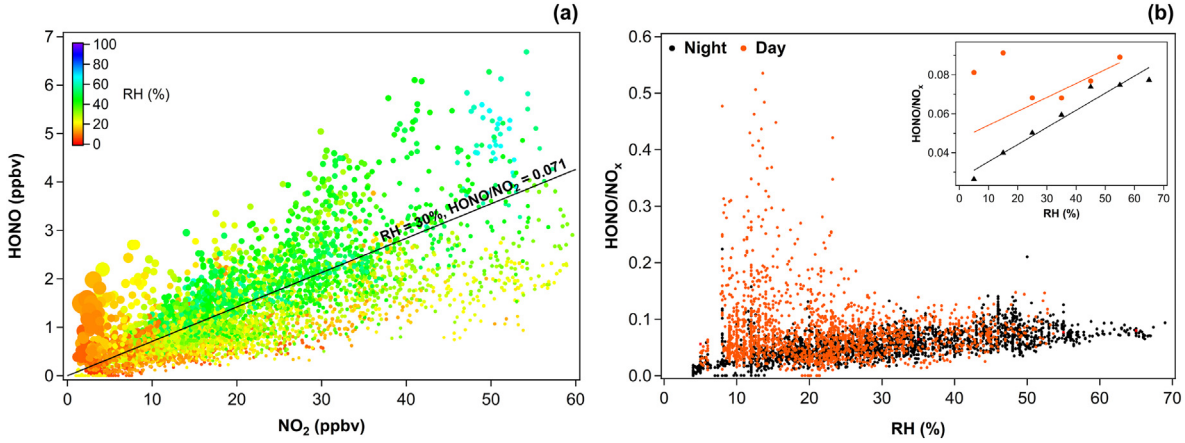

Fig. 5. Scatter plots for data collected in early summer in Beijing. (a) HONO as a function of NO_2 coloured by RH, sized by $HONO/NO_2$, and featuring a trend line of the campaign-average $HONO/NO_2$ ratio; (b) $HONO/NO_x$ as a function of RH, with inset showing the average correlation trends during day and night.

vehicular emission, NO_2 heterogeneous conversion on ground/aerosol surfaces, photo-sensitive NO_2 conversion on ground/aerosol surfaces, and photolysis of pNO_3 contributed 0.21 ppbv h^{-1}, 0.16/0.02 ppbv h^{-1}, 0.25/0.09 ppbv h^{-1}, and 0.02 ppbv h^{-1} of HONO formation, respectively. The significant role of NO + •OH in HONO formation in Beijing was consistent with the recent results reported by Zhang et al. (2019) and Liu et al. (2021). It must be noted that HONO formation from NO + •OH would not increase the net production of atmospheric radicals, while it may increase the radical chain length by preventing chain-termination reactions. These findings highlight the significant role of wintertime photochemistry in megacities, which has usually been neglected in previous studies (Lu et al., 2019).

Fig. 4c–d shows the average diurnal HONO budgets of two typical pollution episodes characterised by heavy aerosol loading in early summer (Episode I) and high NO_x concentration in winter (Episode II). Their budgets were estimated to be similar to those in early summer and winter, both in trend and in proportion. In Episode I, the daytime average $P_{HONO(obs)}$ was 5.59 ± 1.78 ppbv h^{-1}, where the three light-induced sources made the most significant contributions totalling 4.11 ± 0.29 ppbv h^{-1} and collectively accounting for 73.4% of $P_{HONO(obs)}$. This was slightly higher than the average contribution of 65.3% during the early summer; heavier aerosol loading in Episode I along with higher concentrations of NO_2 and pNO_3 accounted for this increased contribution. In Episode II, the daytime average $P_{HONO(obs)}$ was 1.75 ± 1.70 ppbv h^{-1}, which was twice the mean value in winter. The HONO source strength from NO + •OH increased substantially and reached 2.04 ± 0.63 ppbv h^{-1}. Direct emission appeared to be another important source with an average daytime HONO production strength of 0.45 ± 0.08 ppbv h^{-1}. The strong contributions of these two sources was attributed to increased emission intensity, which enhanced the NO and HONO concentrations. In addition, the excessive calculated daytime HONO production rate in Episode II and winter, which featured abundant fresh fuel combustion emissions and relatively weak solar radiation, indicated potentially extra HONO removals.

The upper and lower parameterisation limits in Table 2 were adopted to evaluate the uncertainties in HONO sources. These uncertainties originated from the direct vehicular emission ratio of $HONO/NO_x$ ($ER_{HONO/NOx}$), uptake coefficient of NO_2 on surfaces (γ_{NO2}), and photolysis frequency of pNO_3 ($j(pNO_3)$). In early summer, the parameterisations of direct emission (Fig. S3a) and non-light-related heterogeneous reactions of NO_2 on aerosol (Fig. S3b) and ground surfaces (Fig. S3d) exerted a minor influence on HONO budgets, while the parameterisations of light-related mechanisms dramatically affected daytime HONO source evaluation (Fig. S3c, e and f). With the upper test limits of γ_{NO2} and $j(pNO_3)$, the proportions of light-induced HONO formation rates to $P_{HONO(obs)}$ increased significantly, reaching 260% for $P_{HONO(NO2+h\nu+ground)}$, 36% for $P_{HONO(NO2+h\nu+aerosol)}$, and 42% for $P_{HONO(pNO3+h\nu)}$. However, with the lower test limits of γ_{NO2} and $j(pNO_3)$, the sequentially corresponding proportions dropped to 10.4%, 1.4%, and 1.7%, respectively. As $P_{HONO(NO+•OH)}$ accounted for 8.1% of $P_{HONO(obs)}$, the light-related heterogeneous NO_2 conversion on the ground surface was indicated a larger source of HONO than the NO + •OH reaction, and both light-related NO_2 conversion on the aerosol surface and photolysis of pNO_3 might challenge the contribution of NO + •OH and take over as the other two major sources of daytime HONO, despite that the γ_{NO2} and $j(pNO_3)$ could highly unlikely reach the upper test limits (Yu et al., 2021). We should note that even with a 100% uncertainty of the calculated •OH concentration, the major conclusions of the HONO budget in early summer would not be changed. In winter, γ_{NO2} was the most critical factor influencing the evaluation of daytime HONO sources. The NO + •OH reaction was the dominant HONO source; light-sensitive NO_2 conversion on ground surface (Fig. S3k) was the only pathway that could exceed the dominant contribution of the NO + •OH reaction; light-sensitive NO_2 conversion on aerosol surface (Fig. S3i) and non-light-related NO_2 conversion on ground surface (Fig. S3j) were noted to potentially make considerable contributions but not sufficient to challenge the role of NO + •OH; uncertainties in direct vehicular emission (Fig. S3g), non-light-related NO_2 conversion on aerosol (Fig. S3h), and photolysis of pNO_3 (Fig. S3l) showed negligible influence on HONO source strengths. In addition, considering the large contribution of the NO + •OH reaction to daytime $P_{HONO(obs)}$ in winter, the total calculated HONO source strength could exceed the sink strength, and thus some sink channels were indicated for the budget balance. Besides, we should note that, since the •OH concentration might be overestimated in the fresh wintertime atmosphere, the HONO production rate was possibly subject to overrate. However, even with a half cut in •OH concentration, the NO + •OH was still the major HONO formation pathway and it would not affect the conclusion of this study. In terms of the aforementioned sensitivity results, the conclusions of this work are qualitatively reliable but the quantitative accuracies are still far from optimum, and parametric exactitudes are encouraged to pursue in future studies.

3.3. Contribution to primary •OH production

The sources of primary •OH include HONO photolysis, O_3 photolysis, OVOCs (i.e. oxygenated volatile organic compounds) photolysis, H_2O_2 photolysis, and alkene ozonolysis (Xue et al., 2016). As described in the Introduction, HONO photolysis plays a dominant role in primary •OH formation in most environments. To evaluate the contribution of HONO photolysis to •OH formation in Beijing, we calculated the net primary •OH production rates from photolysis of HONO ($P_{•OH}(HONO)$) and O_3 ($P_{•OH}(O_3)$). Reactions (R1)–(R3) and (R4)–(R6) describe the chemical processes

of primary •OH formation from HONO and O_3, respectively. Eqs. (E2) and (E3) were applied to calculate the $P_{\cdot OH}(HONO)$ and $P_{\cdot OH}(O_3)$, respectively.

$$HONO + h\nu \rightarrow NO + \cdot OH \ (\lambda < 400\ nm) \quad (R1)$$

$$HONO + \cdot OH \rightarrow NO_2 + H_2O \quad (R2)$$

$$NO + \cdot OH + M \rightarrow HONO + M \quad (R3)$$

$$O_3 + h\nu \rightarrow O(^1D) + O_2 \ (\lambda \leq 330\ nm) \quad (R4)$$

$$O(^1D) + H_2O \rightarrow 2 \cdot OH \quad (R5)$$

$$O(^1D) + M \rightarrow O(^3P) + M \ (M = N_2 \text{ or } O_2) \quad (R6)$$

$$P_{\cdot OH}(HONO) = j(HONO)[HONO] - k_{\cdot OH+HONO}[HONO][\cdot OH] - k_{NO+\cdot OH}[NO][\cdot OH] \quad (E2)$$

$$P_{\cdot OH}(O_3) = j(O^1D) \times [O_3] \cdot \frac{2k_{O(^1D)+H_2O}[H_2O]}{k_{O(^1D)+H_2O}[H_2O] + k_{O(^1D)+N_2}[N_2] + k_{O(^1D)+O_2}[O_2]} \quad (E3)$$

Stack plots of the average diurnal $P_{\cdot OH}(HONO)$ and $P_{\cdot OH}(O_3)$ are shown in Fig. 6a–b. HONO photolysis dominated the primary •OH formation in both early summer and winter. The average daytime mean ± sd (maximum) of $P_{\cdot OH}(HONO)$ were 3.86 ± 1.46 (6.47) ppbv h^{-1} in early summer and 0.76 ± 0.46 (1.92) ppbv h^{-1} in winter. In contrast, $P_{\cdot OH}(O_3)$ was only 0.35 ± 0.09 (0.48) ppbv h^{-1} in early summer and negligible in winter. In terms of percentages, $P_{\cdot OH}(HONO)$ accounted for 91.4 ± 3.9% and 99.3 ± 0.6% of $P_{\cdot OH}(HONO)$ + $P_{\cdot OH}(O_3)$ in early summer and winter, respectively. The calculated contribution of HONO photolysis to primary •OH formation in Beijing was at the highest level compared with those in other urban (Li et al., 2018), suburban (Liu et al., 2019b), rural (Gu et al., 2020), and remote sites (Wen et al., 2019). In terms of the diurnal pattern, $P_{\cdot OH}(HONO)$ reached the highest level during the early morning in early summer but around noon in winter. This discrepancy in the time of reaching the maxima should arise from the combined influences of solar intensity and HONO concentration level.

Fig. 6c–d shows stack plots of the average diurnal $P_{\cdot OH}(HONO)$ and $P_{\cdot OH}(O_3)$ in two typical pollution episodes characterised by heavy aerosol loading in early summer (Episode I) and high NO_x concentration in winter (Episode II). As compared with the average rates in these two seasons, the primary •OH production rates increased significantly by up to 3 times in the two episodes. In Episode I, the daytime mean ± sd (maximum) of $P_{\cdot OH}(HONO)$ and $P_{\cdot OH}(O_3)$ were 5.26 ± 2.80 (11.82) ppbv h^{-1} and 0.66 ± 0.22 (1.01) ppbv h^{-1}, respectively; $P_{\cdot OH}(HONO)$ and $P_{\cdot OH}(O_3)$ accounted for 88.8% and 11.2% of $P_{\cdot OH}(HONO)$ + $P_{\cdot OH}(O_3)$, respectively. In Episode II, the daytime $P_{\cdot OH}(HONO)$ was 1.55 ± 1.30 (5.38) ppbv h^{-1}, accounting for 99.7% of $P_{\cdot OH}(HONO)$ + $P_{\cdot OH}(O_3)$, and $P_{\cdot OH}(O_3)$ was almost zero. Photolysis of HONO was the most dominant source of primary •OH in the two episodes, whether under heavy aerosol loading or high NO_x concentration conditions in Beijing. The vital role of HONO in primary •OH formation highlights its significance in atmospheric oxidising capacity and in the establishment of control and mitigation strategies for both haze and photochemical pollutions.

4. Summary and conclusions

In this study, we analysed the HONO characteristics, sources, and impacts on primary •OH during early summer and winter in Beijing. We observed elevated HONO concentrations during both seasons, with the mean ± sd (maximum) of 1.25 ± 0.94 (6.69) ppbv in early summer and 1.04 ± 1.27 (9.55) ppbv in winter. The HONO/NO_x ratio in early summer (0.067 ± 0.042) was twice that in winter (0.031 ± 0.017). Distinct air pollution characteristics were recorded for the two seasons. High degree of ageing and heavy aerosol loading were the main features of early summer (i.e., NO_x/NO_y of 0.60 ± 0.22, $PM_{2.5}$ of 60.0 ± 35.2 μg m^{-3}, and NO_x of 20.7 ± 15.0 ppbv), while abundant fresh fuel combustion emissions, such as NO_x, were the major characteristics of winter (i.e., NO_x/NO_y of 0.87 ± 0.29, $PM_{2.5}$ of 32.4 ± 30.5 μg m^{-3}, and NO_x of 35.0 ± 37.7 ppbv). In addition, the observed daytime HONO source strengths differed between early summer (4.44 ± 1.93 ppbv h^{-1}) and winter (0.88 ± 0.49 ppbv h^{-1}) and the major formation pathways varied between the two seasons as well. In early summer, despite featured heavy aerosol loading, photo-enhanced NO_2 conversion on the ground surface (50.0%) was the most significant HONO source and photo-induced NO_2 conversion on the aerosol surface contributed only 6.9% of the observed HONO formation rate. In winter, which was characterised by abundant fresh emissions, the NO + •OH reaction dominated the HONO formation and accounted for 51.5% of the total calculated HONO production rates. Photolysis of HONO was the governing source of primary •OH in both seasons, with an approximately 10-fold higher contribution than that from photolysis of O_3. This study demonstrates the distinct seasonal variations in air pollution and HONO chemistry in Beijing, underlines the potentially significant role of the NO + •OH reaction in HONO formation, and highlights the dominant role of HONO in atmospheric oxidation across seasons. Our work provides valuable insights for the establishment of strategies for management and prevention of both haze and photochemical pollutions in urban regions.

Data availability

The observation data are available on request from the corresponding authors.

Funding

This work was supported by the National Natural Science Foundation of China (41922051 and 91844301), the Shandong Provincial Science Foundation for Distinguished Young Scholars (ZR2019JQ09), the Hong Kong Research Grants Council (T24-504/17-N), and the Jiangsu Collaborative Innovation Center for Climate Change.

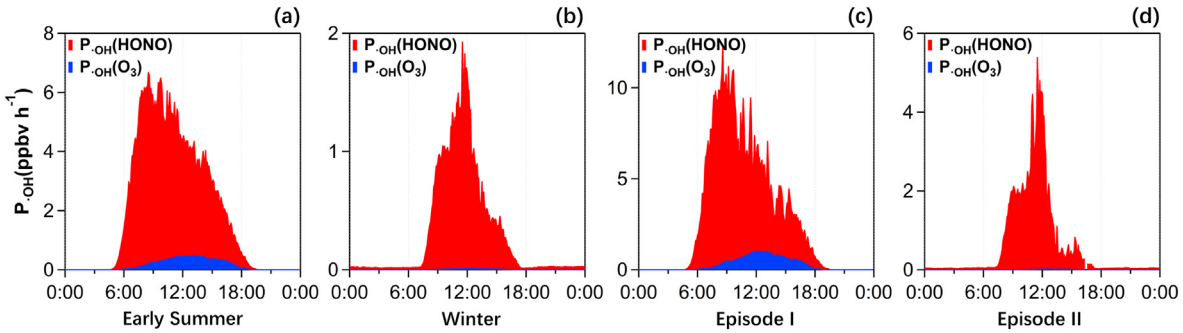

Fig. 6. Stack plots of the net primary •OH production rate in Beijing from the photolysis of HONO and O_3 in (a) early summer, (b) winter, (c) HONO Episode I in early summer (characterised by heavy aerosol loading), and (d) HONO Episode II in winter (characterised by high NO_x concentration).

CRediT authorship contribution statement

Rongrong Gu conducted the HONO measurements, carried out the data analysis, and wrote the manuscript. **Hengqing Shen** participated in the major research discussion and revised the manuscript. **Likun Xue and Tao Wang** designed this study, supervised the analysis, and revised the manuscript. **Jian Gao and Hong Li** arranged the measurements and provided some data. **Yutong Liang, Men Xia, and Chuan Yu** were involved in the field measurements at CRAES. **Yiming Liu** participated in the study discussion and plotted some figures. **Wenxing Wang** supervised this study and provided resources.

Declaration of competing interest

The authors declare that they have no known competing financial interests or personal relationships that could have appeared to influence the work reported in this paper.

Acknowledgements

The authors are grateful to Tsinghua University for offering the MEIC emission inventory.

Appendix A. Supplementary data

Supplementary data to this article can be found online at https://doi.org/10.1016/j.scitotenv.2021.152270.

References

Arens, F., Gutzwiller, L., Baltensperger, U., Gäggeler, H.W., Ammann, M., 2001. Heterogeneous reaction of NO2 on diesel soot particles. Environ. Sci. Technol. 35, 2191–2199. https://doi.org/10.1021/es000207s.

Aumont, B., Chervier, F., Laval, S., 2003. Contribution of HONO sources to the NOx/HOx/O3 chemistry in the polluted boundary layer. Atmos. Environ. 37, 487–498. https://doi.org/10.1016/s1352-2310(02)00920-2.

Barsotti, F., Bartels-Rausch, T., De Laurentiis, E., Ammann, M., Brigante, M., Mailhot, G., Maurino, V., Minero, C., Vione, D., 2017. Photochemical formation of nitrite and nitrous acid (HONO) upon irradiation of nitrophenols in aqueous solution and in viscous secondary organic aerosol proxy. Environ. Sci. Technol. 51, 7486–7495. https://doi.org/10.1021/acs.est.7b01397.

Bejan, I., Abd El Aal, Y., Barnes, I., Benter, T., Bohn, B., Wiesen, P., Kleffmann, J., 2006. The photolysis of ortho-nitrophenols: a new gas phase source of HONO. Phys. Chem. Chem. Phys. 8, 2028–2035. https://doi.org/10.1039/B516590C.

Elshorbany, Y.F., Kleffmann, J., Kurtenbach, R., Lissi, E., Rubio, M., Villena, G., Gramsch, E., Rickard, A.R., Pilling, M.J., Wiesen, P., 2010. Seasonal dependence of the oxidation capacity of the city of Santiago de Chile. Atmos. Environ. 44, 5383–5394. https://doi.org/10.1016/j.atmosenv.2009.08.036.

Finlayson-Pitts, B.J., Pitts, J.N., 2000. Chemistry of the Upper And Lower Atmosphere: Theory, Experiments, And Applications. Academic Press, San Diego. http://www.sciencedirect.com/science/article/pii/B9780122570605500009.

Fu, X., Wang, T., Zhang, L., Li, Q., Wang, Z., Xia, M., Yun, H., Wang, W., Yu, C., Yue, D., Zhou, Y., Zheng, J., Han, R., 2019. The significant contribution of HONO to secondary pollutants during a severe winter pollution event in southern China. Atmos. Chem. Phys. 19, 1–14. https://doi.org/10.5194/acp-19-1-2019.

Gligorovski, S., Strekowski, R., Barbati, S., Vione, D., 2015. Environmental implications of hydroxyl radicals (*OH). Chem. Rev. 115, 13051–13092. https://doi.org/10.1021/cr500310b.

Gu, R., Zheng, P., Chen, T., Dong, C., Wang, Y.n., Liu, Y., Liu, Y., Luo, Y., Han, G., Wang, X., Zhou, X., Wang, T., Wang, W., Xue, L., 2020. Atmospheric nitrous acid (HONO) at a rural coastal site in North China: seasonal variations and effects of biomass burning. Atmos. Environ. 229, 117429. https://doi.org/10.1016/j.atmosenv.2020.117429.

Hao, Q., Jiang, N., Zhang, R., Yang, L., Li, S., 2020. Characteristics, sources, and reactions of nitrous acid during winter at an urban site in the Central Plains Economic Region in China. Atmos. Chem. Phys. 20, 7087–7102. https://doi.org/10.5194/acp-20-7087-2020.

Hastie, D.R., Shepson, P.B., Reid, N., Roussel, P.B., Melo, O.T., 1996. Summertime NOx, NOy, and ozone at a site in rural Ontario. Atmos. Environ. 30, 2157–2165. https://doi.org/10.1016/1352-2310(95)00123-9.

Heland, J., Kleffmann, J., Kurtenbach, R., Wiesen, P., 2001. A new instrument to measure gaseous nitrous acid (HONO) in the atmosphere. Environ. Sci. Technol. 35, 3207–3212. https://doi.org/10.1021/es000303t.

Jiang, Y., Xue, L., Gu, R., Jia, M., Zhang, Y., Wen, L., Zheng, P., Chen, T., Li, H., Shan, Y., Zhao, Y., Guo, Z., Bi, Y., Liu, H., Ding, A., Zhang, Q., Wang, W., 2020. Sources of nitrous acid (HONO) in the upper boundary layer and lower free troposphere of the North China Plain: insights from the Mount Tai Observatory. Atmos. Chem. Phys. 20, 12115–12131. https://doi.org/10.5194/acp-20-12115-2020.

Kanaya, Y., Cao, R., Akimoto, H., Fukuda, M., Komazaki, Y., Yokouchi, Y., Koike, M., Tanimoto, H., Takegawa, N., Kondo, Y., 2007. Urban photochemistry in central Tokyo: 1. Observed and modeled OH and HO2 radical concentrations during the winter and summer of 2004. J. Geophys. Res. Atmos. 112. https://doi.org/10.1029/2007JD008670.

Kleffmann, J., Gavriloaiei, T., 2005. Daytime formation of nitrous acid: a major source of OH radicals in a forest. Geophys. Res. Lett. 32. https://doi.org/10.1029/2005gl022524.

Kurtenbach, R., Becker, K.H., Gomes, J.A.G., Kleffmann, J., Lörzer, J.C., Spittler, M., Wiesen, P., Ackermann, R., Geyer, A., Platt, U., 2001. Investigations of emissions and heterogeneous formation of HONO in a road traffic tunnel. Atmos. Environ. 35, 3385–3394. https://doi.org/10.1016/S1352-2310(01)00138-8.

Li, D., Xue, L., Wen, L., Wang, X., Chen, T., Mellouki, A., Chen, J., Wang, W., 2018. Characteristics and sources of nitrous acid in an urban atmosphere of northern China: results from 1-yr continuous observations. Atmos. Environ. 182, 296–306. https://doi.org/10.1016/j.atmosenv.2018.03.033.

Li, M., Su, H., Li, G., Ma, N., Pöschl, U., Cheng, Y., 2019. Relative importance of gas uptake on aerosol and ground surfaces characterized by equivalent uptake coefficients. Atmos. Chem. Phys. 19, 10981–11011. https://doi.org/10.5194/acp-19-10981-2019.

Li, S., Matthews, J., Sinha, A., 2008. Atmospheric hydroxyl radical production from electronically excited NO2 and H2O. Science 319, 1657–1660. https://doi.org/10.1126/science.1151443.

Liang, Y., Zha, Q., Wang, W., Cui, L., Lui, K.H., Ho, K.F., Wang, Z., Lee, S.-C., Wang, T., 2017. Revisiting nitrous acid (HONO) emission from on-road vehicles: a tunnel study with a mixed fleet. J. Air Waste Manag. Assoc. 67, 797–805. https://doi.org/10.1080/10962247.2017.1293573.

Liu, J., Liu, Z., Ma, Z., Yang, S., Yao, D., Zhao, S., Hu, B., Tang, G., Sun, J., Cheng, M., Xu, Z., Wang, Y., 2021. Detailed budget analysis of HONO in Beijing, China: implication on atmosphere oxidation capacity in polluted megacity. Atmos. Environ. 244. https://doi.org/10.1016/j.atmosenv.2020.117957.

Liu, Y., Lu, K., Li, X., Dong, H., Tan, Z., Wang, H., Zou, Q., Wu, Y., Zeng, L., Hu, M., Min, K.-E., Kecorius, S., Wiedensohler, A., Zhang, Y., 2019a. A comprehensive model test of the HONO sources constrained to field measurements at rural North China Plain. Environ. Sci. Technol. 53, 3517–3525. https://doi.org/10.1021/acs.est.8b06367.

Liu, Y., Nie, W., Xu, Z., Wang, T., Wang, R., Li, Y., Wang, L., Chi, X., Ding, A., 2019b. Semi-quantitative understanding of source contribution to nitrous acid (HONO) based on 1 year of continuous observation at the SORPES station in eastern China. Atmos. Chem. Phys. 19, 13289–13308. https://doi.org/10.5194/acp-19-13289-2019.

Liu, Z., Wang, Y., Costabile, F., Amoroso, A., Zhao, C., Huey, L.G., Stickel, R., Liao, J., Zhu, T., 2014. Evidence of aerosols as a media for rapid daytime HONO production over China. Environ. Sci. Technol. 48, 14386–14391. https://doi.org/10.1021/es504163z.

Lu, K., Fuchs, H., Hofzumahaus, A., Tan, Z., Wang, H., Zhang, L., Schmitt, S.H., Rohrer, F., Bohn, B., Broch, S., Dong, H., Gkatzelis, G.I., Hohaus, T., Holland, F., Li, X., Liu, Y., Liu, Y., Ma, X., Novelli, A., Schlag, P., Shao, M., Wu, Y., Wu, Z., Zeng, L., Hu, M., Kiendler-Scharr, A., Wahner, A., Zhang, Y., 2019. Fast photochemistry in wintertime haze: consequences for pollution mitigation strategies. Environ. Sci. Technol. 53, 10676–10684. https://doi.org/10.1021/acs.est.9b02422.

Ma, Q., Wang, T., Liu, C., He, H., Wang, Z., Wang, W., Liang, Y., 2017. SO2 initiates the efficient conversion of NO2 to HONO on MgO surface. Environ. Sci. Technol. 51, 3767–3775. https://doi.org/10.1021/acs.est.6b05724.

Meusel, H., Kuhn, U., Reiffs, A., Mallik, C., Harder, H., Martinez, M., Schuladen, J., Bohn, B., Parchatka, U., Crowley, J.N., Fischer, H., Tomsche, L., Novelli, A., Hoffmann, T., Janssen, R.H.H., Hartogensis, O., Pikridas, M., Vrekoussis, M., Bourtsoukidis, E., Weber, B., Lelieveld, J., Williams, J., Pöschl, U., Cheng, Y., Su, H., 2016. Daytime formation of nitrous acid at a coastal remote site in Cyprus indicating a common ground source of atmospheric HONO and NO. Atmos. Chem. Phys. 16, 14475–14493. https://doi.org/10.5194/acp-16-14475-2016.

Michoud, V., Colomb, A., Borbon, A., Miet, K., Beekmann, M., Camredon, M., Aumont, B., Perrier, S., Zapf, P., Siour, G., Ait-Helal, W., Afif, C., Kukui, A., Furger, M., Dupont, J.C., Haeffelin, M., Doussin, J.F., 2014. Study of the unknown HONO daytime source at a European suburban site during the MEGAPOLI summer and winter field campaigns. Atmos. Chem. Phys. 14, 2805–2822. https://doi.org/10.5194/acp-14-2805-2014.

Oswald, R., Behrendt, T., Ermel, M., Wu, D., Su, H., Cheng, Y., Breuninger, C., Moravek, A., Mougin, E., Delon, C., Loubet, B., Pommerening-Röser, A., Sörgel, M., Pöschl, U., Hoffmann, T., Andreae, M.O., Meixner, F.X., Trebs, I., 2013. HONO emissions from soil bacteria as a major source of atmospheric reactive nitrogen. Science 341, 1233–1235. https://doi.org/10.1126/science.1242266.

Spataro, F., Ianniello, A., Esposito, G., Allegrini, I., Zhu, T., Hu, M., 2013. Occurrence of atmospheric nitrous acid in the urban area of Beijing (China). Sci. Total Environ. 447, 210–224. https://doi.org/10.1016/j.scitotenv.2012.12.065.

Stemmler, K., Ammann, M., Donders, C., Kleffmann, J., George, C., 2006. Photosensitized reduction of nitrogen dioxide on humic acid as a source of nitrous acid. Nature 440, 195–198. https://doi.org/10.1038/nature04603.

Stutz, J., Alicke, B., Neftel, A., 2002. Nitrous acid formation in the urban atmosphere: gradient measurements of NO2and HONO over grass in Milan,Italy. J. Geophys. Res. Atmos. 107. https://doi.org/10.1029/2001jd000390.

Su, H., Cheng, Y.F., Shao, M., Gao, D.F., Yu, Z.Y., Zeng, L.M., Slanina, J., Zhang, Y.H., Wiedensohler, A., 2008. Nitrous acid (HONO) and its daytime sources at a rural site during the 2004 PRIDE-PRD experiment in China. J. Geophys. Res. Atmos. 113, D14312. https://doi.org/10.1029/2007JD009060.

Sun, L., Chen, T., Jiang, Y., Zhou, Y., Sheng, L., Lin, J., Li, J., Dong, C., Wang, C., Wang, X., Zhang, Q., Wang, W., Xue, L., 2020. Ship emission of nitrous acid (HONO) and its impacts on the marine atmospheric oxidation chemistry. Sci. Total Environ. 735, 139355. https://doi.org/10.1016/j.scitotenv.2020.139355.

Tan, Z., Rohrer, F., Lu, K., Ma, X., Bohn, B., Broch, S., Dong, H., Fuchs, H., Gkatzelis, G.I., Hofzumahaus, A., Holland, F., Li, X., Liu, Y., Liu, Y., Novelli, A., Shao, M., Wang, H., Wu, Y., Zeng, L., Hu, M., Kiendler-Scharr, A., Wahner, A., Zhang, Y., 2018. Wintertime photochemistry in Beijing: observations of ROx radical concentrations in the North

China Plain during the BEST-ONE campaign. Atmos. Chem. Phys. 18, 12391–12411. https://doi.org/10.5194/acp-18-12391-2018.

Tsai, C., Spolaor, M., Colosimo, S.F., Pikelnaya, O., Cheung, R., Williams, E., Gilman, J.B., Lerner, B.M., Zamora, R.J., Warneke, C., Roberts, J.M., Ahmadov, R., de Gouw, J., Bates, T., Quinn, P.K., Stutz, J., 2018. Nitrous acid formation in a snow-free wintertime polluted rural area. Atmos. Chem. Phys. 18, 1977–1996. https://doi.org/10.5194/acp-18-1977-2018.

VandenBoer, T.C., Brown, S.S., Murphy, J.G., Keene, W.C., Young, C.J., Pszenny, A.A.P., Kim, S., Warneke, C., de Gouw, J.A., Maben, J.R., Wagner, N.L., Riedel, T.P., Thornton, J.A., Wolfe, D.E., Dubé, W.P., Öztürk, F., Brock, C.A., Grossberg, N., Lefer, B., Lerner, B., Middlebrook, A.M., Roberts, J.M., 2013. Understanding the role of the ground surface in HONO vertical structure: high resolution vertical profiles during NACHTT-11. J. Geophys. Res. Atmos. 118, 10,155–110,171. https://doi.org/10.1002/jgrd.50721.

Wang, J., Zhang, X., Guo, J., Wang, Z., Zhang, M., 2017. Observation of nitrous acid (HONO) in Beijing, China: seasonal variation, nocturnal formation and daytime budget. Sci. Total Environ. 587–588, 350–359. https://doi.org/10.1016/j.scitotenv.2017.02.159.

Wang, T., Nie, W., Gao, J., Xue, L.K., Gao, X.M., Wang, X.F., Qiu, J., Poon, C.N., Meinardi, S., Blake, D., Wang, S.L., Ding, A.J., Chai, F.H., Zhang, Q.Z., Wang, W.X., 2010. Air quality during the 2008 Beijing Olympics: secondary pollutants and regional impact. Atmos. Chem. Phys. 10, 7603–7615. https://doi.org/10.5194/acp-10-7603-2010.

Wang, T., Poon, C.N., Kwok, Y.H., Li, Y.S., 2003. Characterizing the temporal variability and emission patterns of pollution plumes in the Pearl River Delta of China. Atmos. Environ. 37, 3539–3550. https://doi.org/10.1016/S1352-2310(03)00363-7.

Wang, T., Tham, Y.J., Xue, L., Li, Q., Zha, Q., Wang, Z., Poon, S.C.N., Dubé, W.P., Blake, D.R., Louie, P.K.K., Luk, C.W.Y., Tsui, W., Brown, S.S., 2016. Observations of nitryl chloride and modeling its source and effect on ozone in the planetary boundary layer of southern China. J. Geophys. Res. Atmos. 121, 2476–2489. https://doi.org/10.1002/2015JD024556.

Wen, L., Chen, T., Zheng, P., Wu, L., Wang, X., Mellouki, A., Xue, L., Wang, W., 2019. Nitrous acid in marine boundary layer over eastern Bohai Sea, China: characteristics, sources, and implications. Sci. Total Environ. 670, 282–291. https://doi.org/10.1016/j.scitotenv.2019.03.225.

Wilson, K.R., Smith, J.D., Kessler, S.H., Kroll, J.H., 2012. The statistical evolution of multiple generations of oxidation products in the photochemical aging of chemically reduced organic aerosol. Phys. Chem. Chem. Phys. 14, 1468–1479. https://doi.org/10.1039/C1CP22716E.

Xia, M., Wang, W., Wang, Z., Gao, J., Li, H., Liang, Y., Yu, C., Zhang, Y., Wang, P., Zhang, Y., Bi, F., Cheng, X., Wang, T., 2019. Heterogeneous uptake of N2O5 in sand dust and urban aerosols observed during the dry season in Beijing. Atmosphere 10, 204. https://doi.org/10.3390/atmos10040204.

Xu, Z., Wang, T., Xue, L.K., Louie, P.K.K., Luk, C.W.Y., Gao, J., Wang, S.L., Chai, F.H., Wang, W.X., 2013. Evaluating the uncertainties of thermal catalytic conversion in measuring atmospheric nitrogen dioxide at four differently polluted sites in China. Atmos. Environ. 76, 221–226. https://doi.org/10.1016/j.atmosenv.2012.09.043.

Xue, C., Zhang, C., Ye, C., Liu, P., Catoire, V., Krysztofiak, G., Chen, H., Ren, Y., Zhao, X., Wang, J., Zhang, F., Zhang, C., Zhang, J., An, J., Wang, T., Chen, J., Kleffmann, J., Mellouki, A., Mu, Y., 2020. HONO budget and its role in nitrate formation in the rural North China Plain. Environ. Sci. Technol. 54, 11048–11057. https://doi.org/10.1021/acs.est.0c01832.

Xue, L., Gu, R., Wang, T., Wang, X., Saunders, S., Blake, D., Louie, P.K.K., Luk, C.W.Y., Simpson, I., Xu, Z., Wang, Z., Gao, Y., Lee, S., Mellouki, A., Wang, W., 2016. Oxidative capacity and radical chemistry in the polluted atmosphere of Hong Kong and Pearl River Delta region: analysis of a severe photochemical smog episode. Atmos. Chem. Phys. 16, 9891–9903. https://doi.org/10.5194/acp-16-9891-2016.

Yang, J., Shen, H., Guo, M.-Z., Zhao, M., Jiang, Y., Chen, T., Liu, Y., Li, H., Zhu, Y., Meng, H., Wang, W., Xue, L., 2021. Strong marine-derived nitrous acid (HONO) production observed in the coastal atmosphere of northern China. Atmos. Environ. 244, 117948. https://doi.org/10.1016/j.atmosenv.2020.117948.

Yang, Q., Su, H., Li, X., Cheng, Y., Lu, K., Cheng, P., Gu, J., Guo, S., Hu, M., Zeng, L., Zhu, T., Zhang, Y., 2014. Daytime HONO formation in the suburban area of the megacity Beijing, China. Sci. China Chem. 57, 1032–1042. https://doi.org/10.1007/s11426-013-5044-0.

Ye, C., Gao, H., Zhang, N., Zhou, X., 2016. Photolysis of nitric acid and nitrate on natural and artificial surfaces. Environ. Sci. Technol. 50, 3530–3536. https://doi.org/10.1021/acs.est.5b05032.

Ye, C., Zhang, N., Gao, H., Zhou, X., 2017. Photolysis of particulate nitrate as a source of HONO and NOx. Environ. Sci. Technol. 51, 6849–6856. https://doi.org/10.1021/acs.est.7b00387.

Yokelson, R.J., Crounse, J.D., DeCarlo, P.F., Karl, T., Urbanski, S., Atlas, E., Campos, T., Shinozuka, Y., Kapustin, V., Clarke, A.D., Weinheimer, A., Knapp, D.J., Montzka, D.D., Holloway, J., Weibring, P., Flocke, F., Zheng, W., Toohey, D., Wennberg, P.O., Wiedinmyer, C., Mauldin, L., Fried, A., Richter, D., Walega, J., Jimenez, J.L., Adachi, K., Buseck, P.R., Hall, S.R., Shetter, R., 2009. Emissions from biomass burning in the Yucatan. Atmos. Chem. Phys. 9, 5785–5812. https://doi.org/10.5194/acp-9-5785-2009.

Yu, C., Wang, Z., Ma, Q., Xue, L., George, C., Wang, T., 2021. Measurement of heterogeneous uptake of NO2 on inorganic particles, sea water and urban grime. J. Environ. Sci. 106, 124–135. https://doi.org/10.1016/j.jes.2021.01.018.

Zhang, L., Wang, T., Zhang, Q., Zheng, J., Xu, Z., Lv, M., 2016. Potential sources of nitrous acid (HONO) and their impacts on ozone: a WRF-Chem study in a polluted subtropical region. J. Geophys. Res. Atmos. 121, 3645–3662. https://doi.org/10.1002/2015jd024468.

Zhang, W., Tong, S., Ge, M., An, J., Shi, Z., Hou, S., Xia, K., Qu, Y., Zhang, H., Chu, B., Sun, Y., He, H., 2019. Variations and sources of nitrous acid (HONO) during a severe pollution episode in Beijing in winter 2016. Sci. Total Environ. 648, 253–262. https://doi.org/10.1016/j.scitotenv.2018.08.133.

Zhang, W., Tong, S., Jia, C., Wang, L., Liu, B., Tang, G., Ji, D., Hu, B., Liu, Z., Li, W., Wang, Z., Liu, Y., Wang, Y., Ge, M., 2020. Different HONO sources for three layers at the urban area of Beijing. Environ. Sci. Technol. 54, 12870–12880. https://doi.org/10.1021/acs.est.0c02146.

Zhou, X., Huang, G., Civerolo, K., Roychowdhury, U., Demerjian, K.L., 2007. Summertime observations of HONO, HCHO, and O3 at the summit of Whiteface Mountain, New York. J. Geophys. Res. Atmos. 112. https://doi.org/10.1029/2006JD007256.